

Jiaqing Kou^{1,2,3}, Chenjia Ning^{1,2,3} & Weiwei Zhang^{1,2,3}

¹School of Aeronautics, Northwestern Polytechnical University, Xi'an, 710072, China ²International Joint Institute of Artificial Intelligence on Fluid Mechanics, Northwestern Polytechnical University, Xi'an, 710072, China

³National Key Laboratory of Aircraft Configuration Design, Xi'an 710072, China

Abstract

Reduced-order modeling for multi-fidelity flow reconstruction enhances accuracy while reducing the costs associated with data generation. The success of multi-fidelity models hinges on accurately capturing the correlations between low- and high-fidelity data. In this work, we propose the use of transfer learning to identify representative features that more effectively correlate the multi-fidelity data, thereby improving the accuracy of multi-fidelity flow reconstruction. Essentially, transfer learning aids the modeling process by applying knowledge acquired from related tasks, thus enhancing performance in multi-fidelity scenarios. Specifically, we introduce a common class of transfer learning based on domain adaptation to uncover domain-invariant features from flow data across multiple sources. We establish two transfer learning frameworks, either through transfer component analysis or geodesic flow kernel, each offering distinct approaches to align transferred features across multi-fidelity data. These transferred features are then utilized to construct the bridge function between low- and high-fidelity data for flow reconstruction. The proposed transfer learning methods have been validated by two test cases, including transonic flows past a NACA0012 airfoil and an ONERA M6 wing. We present the advantages of our transfer learning approach in achieving superior feature representations and in facilitating the construction of more accurate multi-fidelity models for flow reconstruction.

Keywords: Transfer Learning; Unsteady Flow; Machine Learning; Reduced-Order Model

1. Introduction

In recent years, the generation of massive big data in experiment and simulation of fluid dynamics has opened many possibility for the development of data-driven flow models [1, 2, 3]. Traditionally, most of the research in flow reconstruction builds aerodynamic ROMs from a single source of data. However, the generated unsteady flow data are multi-source and multi-fidelity in nature. Depending on their source and acquisition methods, flow field data themselves vary in accuracy, computational cost, and difficulty of generation. Particularly, flow data can be obtained from flight test, experiment, simulation, theoretical models, etc. Therefore, the desire of modeling flow dynamics from multi-source data has motivated the research in data fusion [4] and multi-fidelity methods [5, 6]. Through combining low-fidelity and high-fidelity data, the model accuracy can be increased while the overall computational cost is reduced.

For complex flow problems such as high angle-of-attack stall and transonic flow, the comprehensive utilization of data from different sources can significantly reduce modeling cost and enhance the reliability of aerodynamic models. To develop data fusion aerodynamic models, traditional methods mainly focus on steady aerodynamics research, such as Co-Kriging models, etc. Recently, Kou and Zhang [7] have proposed data fusion model frameworks for unsteady aerodynamics, achieving multifidelity modeling for airfoil in transonic flows under high angles of attack with a small amount of flow data. For multi-fidelity flow field modeling, Wang et al. [8] have proposed the framework that first uses Proper Orthogonal Decomposition (POD) to reduce the dimensionality of high-fidelity and low-fidelity

flow fields, and then constructs a mapping between the modal coefficients of high-fidelity and low-fidelity data. This conventional multi-fidelity flow field modeling methods mentioned above directly establish a mapping for high-fidelity flow field features, without further considering the correlation between multi-fidelity samples.

Transfer learning [9, 10, 11, 12] is a typical machine learning method, offering a series of ideas and specific algorithms to extend the knowledge learned in a specific domain (source domain) to a new target domain, thereby improving the performance in the target domain. Essentially, the idea of transfer learning mainly comes from the human learning progress, i.e., applying existing knowledge to solve a new problem in order to improve efficiency and achieve better results. More details on transfer learning can be found in Pan and Yang [9]. In fluid mechanics, existing flow models can be transferred to new but related problems, leading to two potential applications: 1) transferring the model from one parameter range to another (model calibration); 2) transferring low-fidelity data to match the features of high-fidelity data (data calibration). The former has been studied through fine-tuning the neural network for modeling fluid dynamics. However, the other type of transfer learning based on domain adaptation for multi-fidelity flow reconstruction remains unexplored, which is the focus of the present paper. In the framework of transfer learning, the low-fidelity sample space defines the source domain, while the high-fidelity sample space defines the target domain. Transfer learning introduces a particular mapping that transforms high-fidelity and low-fidelity data into a more consistent feature space, further establishing a new architecture for multi-fidelity flow field reconstruction.

To accurately capture the correlation between multi-fidelity flow data, reduced-order modeling framework for flow reconstruction is constructed by transfer learning. Using two domain-adaptation-based transfer learning methods, the difference in feature distribution between the low-fidelity source domain and high-fidelity target domain is reduced, thus obtaining more representative low-fidelity features. Thereafter, the transferred features can be used as inputs to build the multi-fidelity model, to obtain the high-fidelity mode coefficient and reconstructing the high-fidelity flows. A schematic illustration of the proposed methods and the standard POD-based multi-fidelity method [8] is shown in Fig. 1, which shows the difference between different methods, and will be detailed in the next section. The figure clearly shows that the traditional standard method directly establishes a model between the POD coefficients of high-fidelity and low-fidelity samples. The proposed two transfer learning methods include: 1) Transfer Component Analysis (TCA), which transforms the features after POD dimensionality reduction; 2) Geodesic Flow Kernel (GFK), which directly transforms the high and low precision flow snapshots. The proposed methods and test cases will be introduced below.

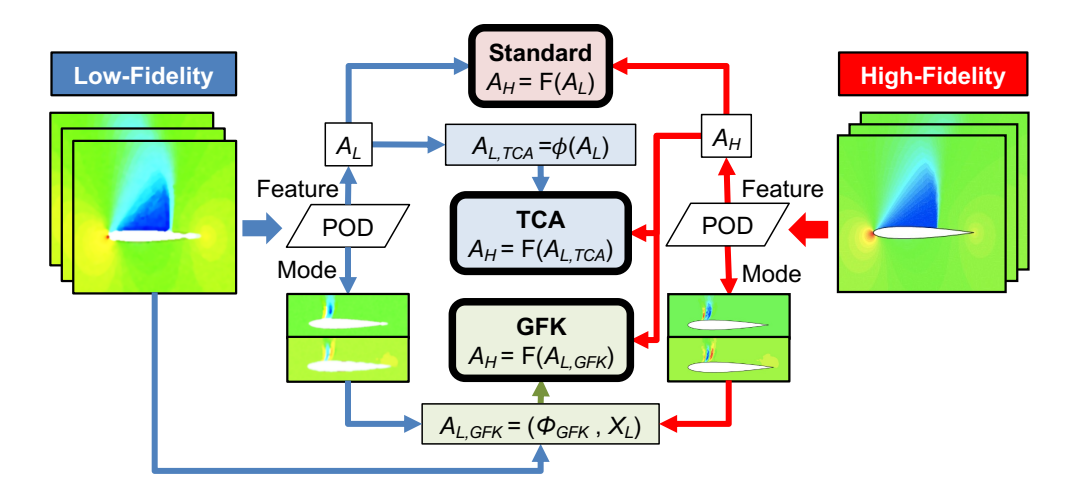


Figure 1 – Schematic illustration of the standard method, and the proposed transfer learning approaches for flow reconstruction based on multi-fidelity data.

2. Transfer Learning based on Domain Adaptation

The basic idea to use transfer learning for flow reconstruction is to determine a good feature representation that can minimize the discrepancy of feature distributions between low-fidelity and high-fidelity

domains, while maintaining important features in each domain [13]. To this end, domain adaptation techniques [14, 15, 16] are introduced here for the transfer learning task, which correct the mismatch in statistical properties of features in the source domain and the target domain. For example, in a classification problem, domain adaptation enables the generalization of the classifier learned in the source domain to the target domain [17].

In domain adaptation, each domain has two components: input feature space χ and marginal probability distribution of the input P(X), where X is the feature data set containing a set of learning samples. Given one source domain \mathcal{D}_S and one target domain \mathcal{D}_T , domain adaptation problem is formulated as [13]: the source domain has input features x_S and output labels y_S , i.e., $\mathcal{D}_S = \{(x_{S_1}, y_{S_1}), ..., (x_{S_{n1}}, y_{S_{n1}})\}$; the target domain only contains features x_T , while the input and output features satisfy x_S , $x_T \in \chi$. Note that if domain adaptation is used for unsupervised learning problems, labels in the source domain are not needed. The marginal distributions $\mathcal{P}(X_S)$ and $\mathcal{P}(X_T|Y_T)$ in the source and target domains can be different, while the conditional probabilities $P(X_S|Y_S)$ and $P(X_T|Y_T)$ are assumed to be similar. With these assumptions, the shared features can be found through transfer learning to match the feature distributions of the source domain and the target domain.

2.1 Transfer Component Analysis

TCA [13] is a domain adaptation transfer learning method that utilizes dimensionality reduction techniques. For situations where the data distributions of the source and target domains differ, TCA maps both types of data into a common space. To achieve this, TCA first introduces kernel tricks to perform nonlinear transformations of features. In the transformed space, it minimizes the differences between the source and target domains. Furthermore, additional constraints are introduced to maintain the characteristics of the original data within their respective regions. TCA ultimately obtains a transformation matrix, which is used to further transform any new sample's mapping in the kernel space into the feature space. The basic concept is illustrated in Fig. 2a, while more details can be found in [13].

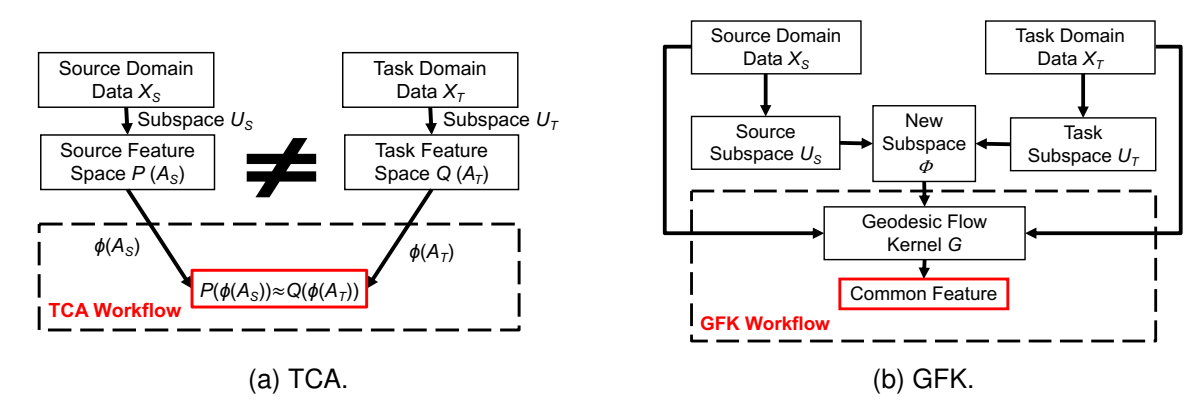


Figure 2 – Basic concepts of TCA and GFK.

2.2 Geodesic Flow Kernel

GFK is a domain adaptation method based on subspaces, which directly transforms samples into a new subspace. As this subspace is an invariant feature space concerning both the source and target domains, the data from these domains exhibit high similarity. GFK utilizes the concept of high-dimensional manifold spaces, considering the source and target domains as two states on the Grassmann manifold. By constructing a geodesic flow between these two points and integrating along this geodesic, a domain-invariant subspace is obtained. Projecting the original high-dimensional snapshots into this subspace achieves the transfer of information. The basic concept is illustrated in Fig. 2b, while more details can be found in [18, 19].

3. Transfer Learning for Flow Reconstruction

In recent years, flow reconstruction based on multi-fidelity data has gained more attentions [20, 8, 21]. Currently, dimensionality reduction via POD is usually used as the first step to obtain low-dimensional subspaces (corresponds to flow modes) and features (corresponds to mode coefficient).

Note that nonlinear dimeisonality reduction methods (e.g., neural networks) can also be used to extract low-dimensional representations [22]. Using this modal information, two ideas are generally followed: 1) constructing a nonlinear mapping / bridge function between low-fidelity and high-fidelity mode coefficients [20, 8]; 2) matching low-fidelity features to fit high-fidelity data, like the manifold alignment [21]. The current work follows the former one. However, the low-fidelity features are not directly obtained from low-fidelity mode coefficients but from more representative features using transfer learning (TCA and GFK).

3.1 Basic Ideas

The first step for flow reconstruction usually starts from mode decomposition, to reduce the dimension of the high-dimensional flow data and extract the dominant flow features. Any high-dimensional flow snapshot $x \in R^m$ can be represented as the following expansion:

$$\mathbf{x} = \sum_{i=1}^{r} a_i(\boldsymbol{\theta}) \boldsymbol{\phi}_i, \tag{1}$$

where ϕ is the flow mode and a is the coefficient of each mode. The mode coefficient is a function of parameter θ , e.g., flow state or time. This linear mode decomposition is in generally achieved by POD or DMD, where DMD is related to unsteady problems and POD is a purely dimensionality reduction method. Here we consider POD for the generalization of both steady and unsteady flows: given flow snapshot matrix $\mathbf{X} \in R^{m \times n}$ containing each snapshot as a column, POD performs SVD to \mathbf{X} : $\mathbf{X} = \mathbf{U} \mathbf{\Sigma} \mathbf{V}^T$, where the flow mode corresponds to matrix \mathbf{U} and mode coefficient corresponds to the remaining part . Dominant modes are ranked and retained based on the mode energy indicator defined as the singular value contained in $\mathbf{\Sigma}$.

For multi-fidelity modeling, given the high-fidelity and low-fidelity flow snapshots $\mathbf{X}_L \in R^{m \times n_1}, \mathbf{X}_H \in R^{q \times n_2}$, the modal expansions can be obtained from each dataset:

$$\boldsymbol{X}_{L} = \boldsymbol{\Phi}_{L} \boldsymbol{A}_{L}, \quad \boldsymbol{X}_{H} = \boldsymbol{\Phi}_{H} \boldsymbol{A}_{H}, \tag{2}$$

where Φ_L and Φ_H are the modes of low-fidelity and high-fidelity flows, respectively. A_L and A_H are the vectors containing their corresponding mode coefficients. When only high-fidelity flow data is available, the ROM is constructed from a nonlinear mapping between the state variable θ and the mode coefficients a_H after POD, i.e., $a_H = g(\theta)$. The motivation of multi-fidelity modeling is to improve the prediction of high-fidelity flows through using the corresponding low-fidelity counterparts (usually at the same flow state but are obtained with reduced fidelity and cost). In the context of transfer learning, low-fidelity data X_L is the source domain data X_S , and the high-fidelity data X_H is the target domain data X_T . Transfer learning aims at discovering the mapping to transfer the source domain information thus improving the modeling accuracy in the target domain, which is the main motivation of the present work. In the proposed methods, transfer learning performs unsupervised learning to obtain feature transformation for low-fidelity data that are more consistent with high-fidelity samples, resulting in more accurate ROMs.

A brief analysis in the context of domain adaptation is provided here to justify the use of transfer learning for multi-fidelity flow reconstruction. Since the latent space where the high-fidelity and low-fidelity samples lie is determined by their respective POD bases, the marginal distribution between the two samples can be different, i.e, $\mathscr{P}(X_L) \neq \mathscr{Q}(X_H)$. Moreover, the difference in mode coefficients (i.e., labels or features) leads to different conditional distributions $P(A_L|X_L)$ and $P(A_H|X_H)$. The goal of using TCA or GFK is to match the marginal distributions: $\mathscr{P}(\phi(X_L)) \approx \mathscr{Q}(\phi(X_H))$, thus making the conditional distribution similar: $P(A_L|\phi(X_L)) \approx P(A_H|\phi(X_H))$.

3.2 Basic Algorithm

The basic algorithm of multi-fidelity modeling is inherited from previous research, i.e., the low-fidelity features are mapped to high-fidelity features (at the same flow states), and the predicted high-fidelity features are used for flow reconstruction. Previous works directly map the high-fidelity and low-fidelity mode coefficients [20, 8]:

$$a_H = g(a_L), (3)$$

where g is the surrogate model for nonlinear mappings between mode coefficients (also known as the bridge function [23]). However, due to the differences in the latent space of high-fidelity and low-fidelity data, such a direct mapping can be inaccurate. The present work tries to discover more representative low-fidelity information with respect to high-fidelity features to handle this potential drawback. Through transfer learning, the following mapping is constructed:

$$a_H = g(a_{L, \text{method}}), \tag{4}$$

where $a_{L, \text{method}}$ refers to the transferred low-fidelity features, and 'method' refers to TCA or GFK. The transferred low-fidelity features can be more consistent with high-fidelity features, thus a simpler bridge function with improved accuracy can be obtained (compared to Eq. 3). As discussed in the previous section, TCA focuses on matching the features (i.e., the transfer of mode coefficient), while GFK method focuses on transferring the data (i.e., the transformation of flow snapshot) to the domain-invariant space. It is worth noting again that when g is being identified, the sample pairs $(a_{L, \text{method}}, a_H)$ usually correspond to the same flow parameter θ (which also applies to standard multifidelity methods). In summary, a schematic illustration of different multi-fidelity models, including the standard method (Eq. 3), the TCA and the GFK methods, is shown in Fig. 1. It can be observed that the proposed method aims to obtain new features from the low-fidelity data to reflect the high-fidelity flow dynamics, while the difference between TCA and GFK lies on which information is needed for transfer learning. The developed transfer learning frameworks for flow reconstruction will be detailed as follows.

3.2.1 TCA: Transferring Low-dimensional Features (Mode Coefficient)

Transfer learning for flow reconstruction based on TCA aims to determine nonlinear transformations for high-fidelity (target domain) and low-fidelity (source domain) mode coefficients, to ensure that the transformed data distributions are similar. The model framework, including offline training and online predicting steps, are summarized in **Algorithm 1** and illustrated in Fig. 3.

Algorithm 1 Transfer learning framework for flow reconstruction based on TCA.

Offline Phase (Model Training):

- 1: Sampling in the parameter space to obtain low-fidelity and high-fidelity flow data;
- 2: Performing dimensionality reduction using POD, to obtain low-fidelity and high-fidelity flow features (mode coefficients) respectively;
- 3: Performing TCA on features A_L and A_H to get the transformation matrix W (see);
- 4: Converting the low-fidelity mode coefficients to the transferred space $(\mathbf{A}_{L,TCA} = \mathbf{k}_{\mathbf{A}_L}^T \mathbf{W})$ to get $\mathbf{A}_{L,TCA}$;
- 5: Constructing the bridge function g between $A_{L,TCA}$ and A_H .

Online Phase (Prediction):

- 1: Selecting the flow parameter θ^* for test case and computing the low-fidelity flow field x_L^* ;
- 2: Obtaining the low-fidelity mode coefficients $\boldsymbol{a}_{L}^{*} = \boldsymbol{\Phi}_{L}^{T} \boldsymbol{x}_{L}^{*}$;
- 3: Converting a_L^* to the transferred space to get $a_{L,TCA}^*$ (see Step 4 in the offline phase);
- 4: Predicting the high-fidelity mode coefficient $\mathbf{a}_H^* = g(\mathbf{a}_{L,TCA}^*)$ through g, and reconstructing the high-fidelity flow field via $\mathbf{x}_H^* = \mathbf{\Phi}_H \mathbf{a}_H^*$.

3.2.2 GFK: Transferring Flow Snapshots

GFK-based transfer learning aims at obtaining a snapshot transformation matrix that transfers all snapshots to a domain-invariant feature space. Since both the high-fidelity and the low-fidelity flow snapshots need to be transferred using the same transformation matrix, the dimensions of high-fidelity and low-fidelity snapshots need to be the same. The model framework, including offline training and online predicting steps, is summarized in **Algorithm 2** and illustrated in Fig. 4.

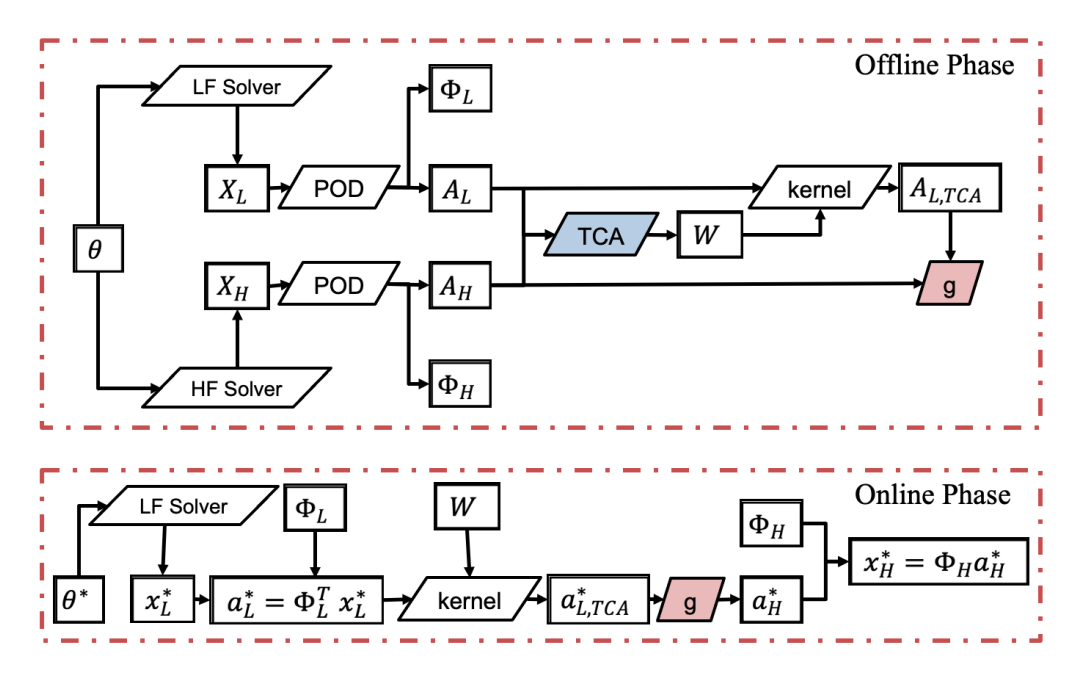


Figure 3 – Flowchart of transfer learning framework for flow reconstruction based on TCA.

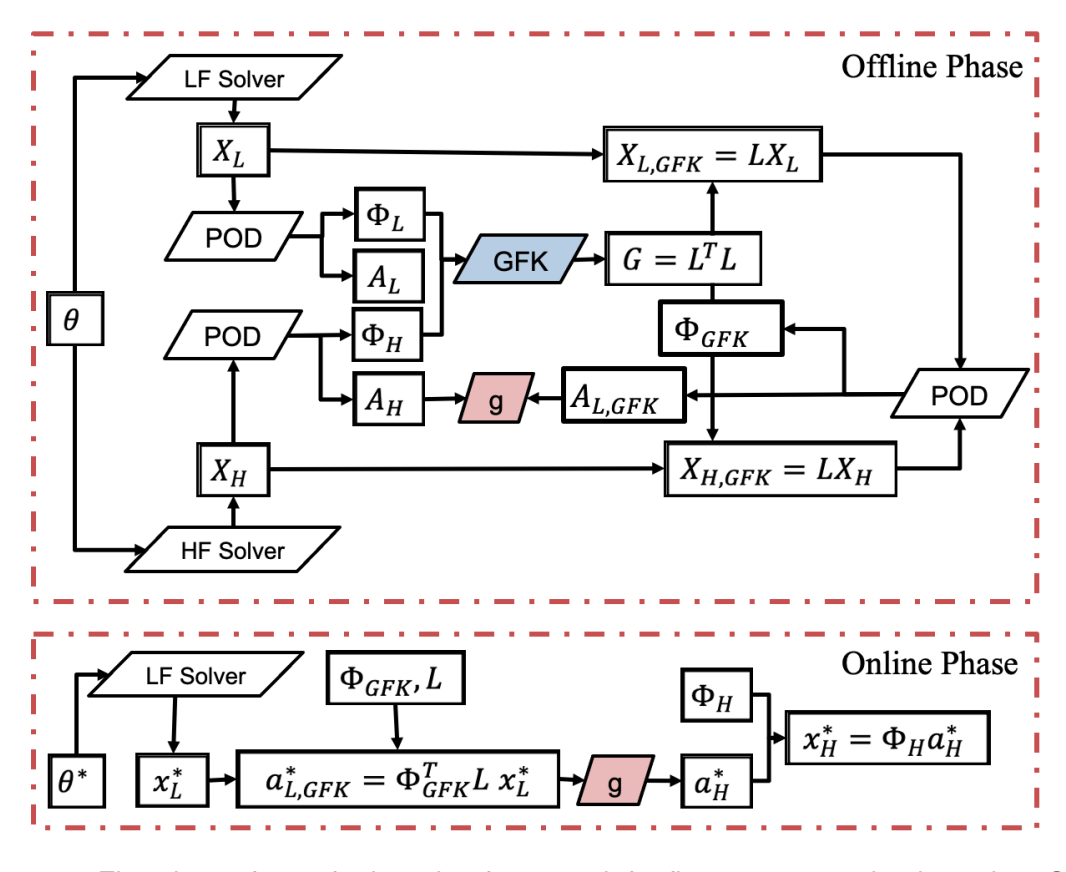


Figure 4 – Flowchart of transfer learning framework for flow reconstruction based on GFK.

Algorithm 2 Transfer learning framework for flow reconstruction based on GFK.

Offline Phase (Model Training):

- 1: Sampling in the parameter space to obtain low-fidelity and high-fidelity flow data;
- 2: Performing POD to get modal information for low-fidelity and high-fidelity flow data, respectively;
- 3: Performing GFK on low-fidelity and high-fidelity flow modes Φ_L and Φ_F , in order to obtain the geodesic flow kernel matrix G (thus computing L);
- 4: Transforming the low-fidelity and high-fidelity snapshots as $X_{L,GFK} = LX_L, X_{H,GFK} = LX_H$;
- 5: Performing POD on the transformed snapshots (including both low-fidelity and high-fidelity data), and obtaining the transformed mode Φ_{GFK} and the corresponding mode coefficient $A_{L.GFK}$ for low-fidelity dataset;
- 6: Constructing the bridge function g between $\mathbf{A}_{L,GFK}$ and \mathbf{A}_{H} .

Online Phase (Prediction):

- 1: Selecting the flow parameter θ^* for test case and computing the low-fidelity flow field x_L^* ;
- 2: Using transformed mode Φ_{GFK} and matrix L to calculate the transformed low-fidelity mode coefficient $a_{L,GFK}^* = \Phi_{GFK}^T L x_L^*$;
- 3: Predicting the high-fidelity mode coefficient $\boldsymbol{a}_H^* = g(\boldsymbol{a}_{L,GFK}^*)$ through g, and reconstructing the flow field via $\boldsymbol{x}_H^* = \boldsymbol{\Phi}_H \boldsymbol{a}_H^*$.

3.3 Interpolation Method

The bridge function *g* between low-fidelity and high-fidelity features can be constructed through different interpolation methods. Using transfer learning, the distribution properties between multi-fidelity data become closer to each other, thus improving the model performance. The input features used for interpolation are determined in a case-by-case manner, depending on the complexity of the problem. For flow over airfoils and wings, nonlinear interpolation method is used to construct a multiple-to-one mapping, such as the Kriging interpolation [24]. The general formulation of Kriging is as follow:

$$g(x) = f(x) + z(x), \tag{5}$$

where f is the regression polynomial model and z is the stochastic process term. The regression model provides the global trend function, while the stochastic process reflects the local deviations. In the present work, the Kriging method is implemented in the Matlab Toolbox DACE [25]. For both examples, the polynomial order of the Kriging model is set to 1. The correlation functions are selected based on a combined trial-and-error and cross-validation approach, where either Gaussian or linear functions are used. Hyperparameters of the model are determined by solving an optimization problem with box constraints [25], whose range is set between 1×10^{-8} and 100. Note that the selection of Kriging functions is problem dependent and can vary case-by-case. Details in the method are described in Wang et.al [8]. The identification of bridge function g is the last step in the offline phase of the proposed framework.

4. Test Case

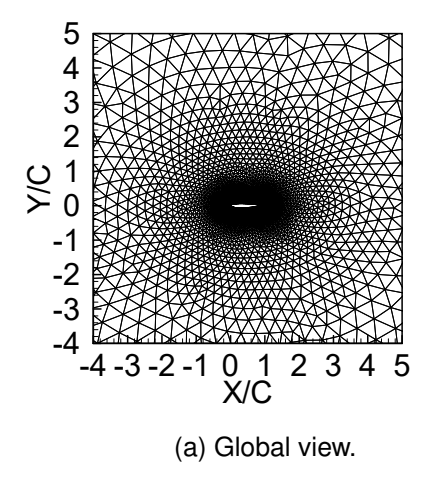
In this section, the proposed transfer learning methods for flow reconstruction are tested by two cases: 1) transonic flow past a NACA0012 airfoil; 2) transonic flow past an ONERA M6 wing. For each test case, low-fidelity solutions are obtained by less accurate numerical methods or a relaxed convergence criterion. Two test cases are summarized in Table 1. For comparison purposes, additional ROMs are also introduced, resulting in four different models including:1) High-Fidelity: Using only high-fidelity samples to build model $a_H = g(\theta)$, without considering multi-fidelity data; 2) Standard: Directly constructing the bridge function between high-fidelity and low-fidelity mode coefficients, $a_H = g(a_{L,TCA})$; 4) GFK: Using the GFK features to predict high-fidelity mode coefficients, $a_H = g(a_{L,GFK})$.

Table 1 – Two test cases introduced in the present paper.

Case	High-Fidelity Data	Low-Fidelity Data	Parameter	Parameter Range	
A. Transonic Flow	Second-order	First-order	Angle of attack	$\alpha \in [-2^{\circ}, 6^{\circ}],$	
over a NACA0012	flux reconstruc-	flux reconstruc-	α , Mach num-	$Ma \in [0.7, 0.8]$	
Airfoil	tion	tion	ber Ma		
B. Transonic Flow	Convergence	Convergence	Angle of attack	$lpha \in [0^\circ, 5^\circ],$	
over an ONERA	criterion 1×10^{-6}	criterion 1×10^{-1}	α , Mach num-	$Ma \in [0.78, 0.84]$	
M6 Wing			ber Ma		

4.1 NACA0012 Airfoil

To test the proposed method in a more realistic flow problem, this section presents transonic flow reconstruction for pressure field of flow over a NACA0012 airfoil. This test case is taken from Wang et al. [8], which is challenging due to the existence of shock wave that creates discontinuities in the solution. The inviscid Euler equations are solved by the in-house flow solver [26, 27]. based on unstructured grid and finite volume scheme. The computational grid is shown in Fig.5, which contains 6916 nodes and 13490 elements and C is the chord length. Here the low-fidelity flows are generated based on first-order scheme for flux reconstruction, while the high-fidelity data are calculated based on second-order scheme for flux reconstruction.



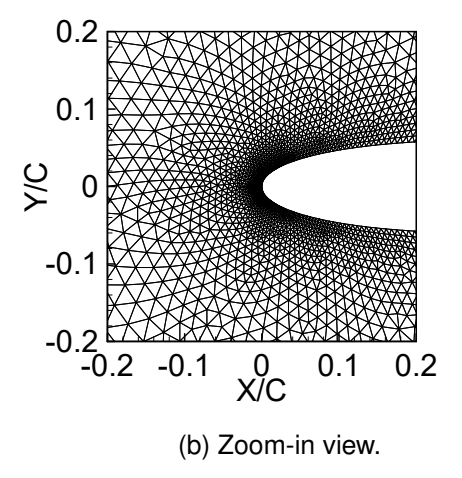


Figure 5 – Computational grid for transonic flow around a NACA0012 airfoil.

This test case aims at reconstructing steady flow field in a two-dimensional parameter space composed of the angle of attack α and Mach number Ma. The sampling ranges are fixed to $Ma \in [0.7, 0.8]$ and $\alpha \in [-2^{\circ}, 6^{\circ}]$, and 28 training cases are selected based on the Latin hypercube sampling [28]. In addition, two typical states at $(\alpha, Ma) = (3.7377^{\circ}, 0.7186)$ and $(\alpha, Ma) = (4.5219^{\circ}, 0.7525)$ are selected to test the interpolation performance and one state outside the parameter space $(\alpha, Ma) = (1.0173^{\circ}, 0.8042)$ is selected for extrapolation purpose. All sampling points are shown in Fig. 6. To fully evaluate the model performance, other 6 test cases are also included when computing the average prediction error and error contours. This results in a total number of 9 test cases. Fig. 7a compares the surface distribution of pressure coefficient for a typical training case at $(\alpha, Ma) = (4.8217^{\circ}, 0.7137)$. Apparently, the low-fidelity results are less smooth near the leading edge, and the strength and position of shock wave are misrepresented compared to high-fidelity results.

Different from previous work [8] where the high-dimensional flow is directly defined as the snapshot, the present ROM is constructed only from surface pressure data. This is because obtaining matrix G in the GFK method is time consuming since the matrix size scales with the snapshot dimension, and its square root matrix L needs to be solved. This computational issue can be regarded as a limitation of the standard GFK method, which needs to be improved in future works. Therefore, the snapshot

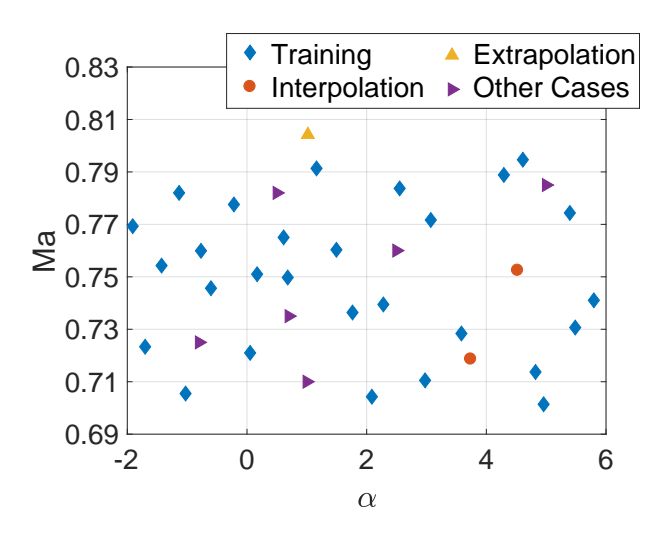


Figure 6 – Sampling space for transonic flow around a NACA0012 airfoil.

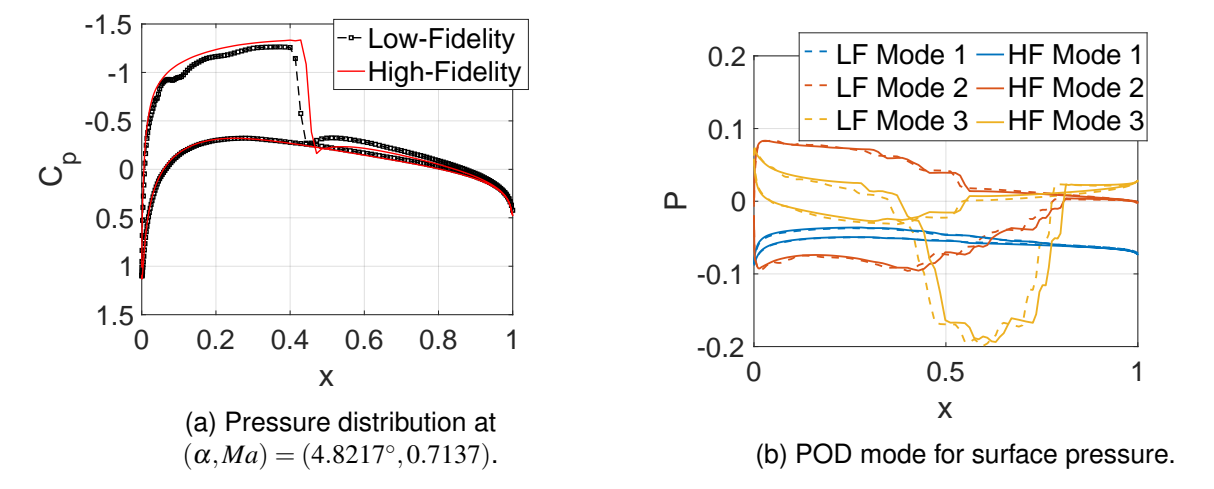


Figure 7 – Comparison of low-fidelity and high-fidelity solutions of transonic flow around a NACA0012 airfoil.

matrix only contains pressure on the surface, defined as $X_{H,surface}$ and $X_{L,surface}$ for high-fidelity and low-fidelity data, respectively. The snapshot dimension becomes 300 since there are 300 points on the surface of airfoil. However, using the reconstructed surface pressure distribution, the global flow field X can still be reconstructed through the global POD basis Φ :

$$\mathbf{X}_{H} = \mathbf{\Phi}_{H} \mathbf{a}_{H}, \ \mathbf{a}_{H} = (\mathbf{\Phi}_{H.\text{surface}})^{+} \mathbf{X}_{H.\text{surface}},$$
 (6)

where '+' represents the pseudo-inverse of the matrix, and $\Phi_{H,\text{surface}}$ corresponds to the mode values of Φ_H on the surface. This idea of reconstruction comes from gappy POD [29], discrete empirical interpolation method [30] and the sparse reconstruction method [31], to recover the entire flow through partial flow data that are sparse in space. This reconstruction greatly helps to reduce the computational effort in transfer learning when the dimension of data is high. Since TCA focuses on the low-dimensional features which scale with the dimension of the reduced subspace, the dimension of snapshot does not affect its efficiency. Fig. 7b shows the difference between high-fidelity and low-fidelity modes on the surface pressure data. Compared to one-dimensional test cases, the present test case is more complicated since there is a greater difference between the high-fidelity and low-fidelity modes. For example, due to the difference in shock wave positions (as shown in Fig. 7a), high-order modes are different near the shock, such as the third-order POD mode compared in Fig. 7b.

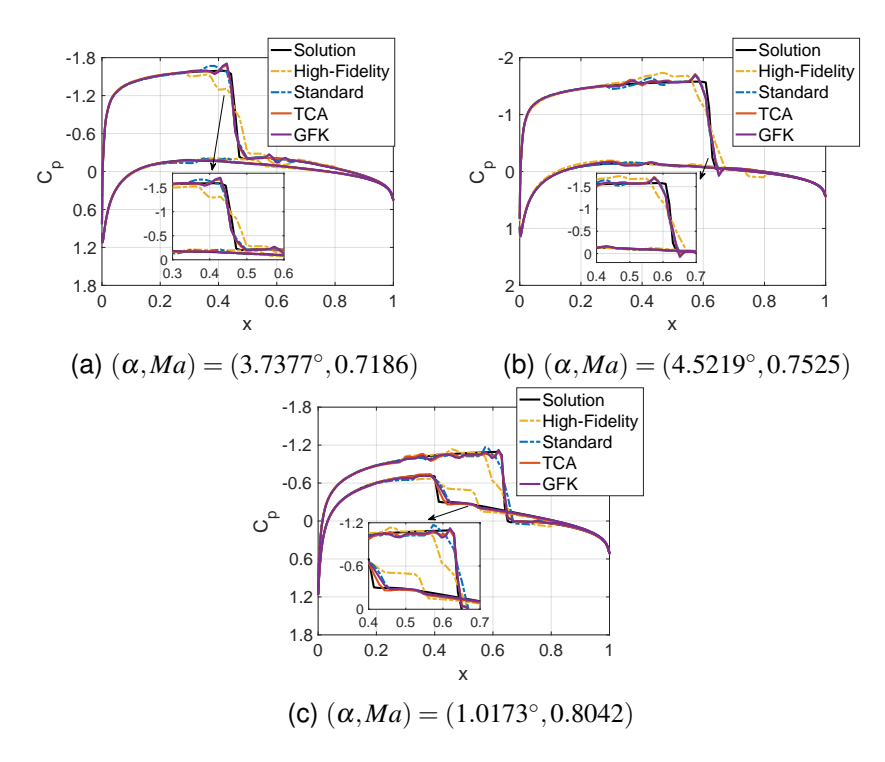


Figure 8 – Reconstructed surface pressure distribution for transonic flow around a NACA0012 airfoil (two interpolation cases and one extrapolation case).

When constructing high-fidelity ROM for comparison purposes, state parameters are selected as the model input, including the angle of attack and the Mach number. Due to the complexity in transonic flows, multiple low-fidelity features are needed to predict each high-fidelity feature, despite the use of transfer learning. Kriging interpolation is used as the bridge function for all methods. From Wang et al. [8], when the number of input features are more than 10, high prediction accuracy can be obtained. To make a fair comparison among all methods, all multi-fidelity models should use the same number of input features. From one-dimensional test cases, transfer learning enables extracting a deeper correlation between high-order features, therefore the first 18 low-fidelity features are selected as the input for all multi-fidelity methods (including Standard, TCA and GFK). The model is used to recover the first 20 POD coefficients of the high-fidelity data. Additionally, the present work aims to show the potential of transfer learning in multi-fidelity flow reconstruction, while some detailed studies

Table 2 – Prediction error of surface pressure reconstruction by different methods (9 test cases, NACA0012 airfoil).

Method	Mean	Standard Deviation
High-Fidelity	1.0895×10^{-2}	1.9835×10^{-2}
Standard	4.9292×10^{-3}	1.3441×10^{-2}
TCA	3.9566×10^{-3}	1.1198×10^{-2}
GFK	4.0002×10^{-3}	1.1440×10^{-2}

remain unexplored, such as the judicious selection of the kernel function in TCA and the possibility of nonlinear kernels in GFK, which may further improve the model performance.

Fig. 8 shows the reconstructed surface pressure coefficient of three test cases, including two for interpolation and one for extrapolation. In general, the reconstruction error mainly exists in the vicinity of the shock wave, due to its highly nonlinear nature. Through transfer learning, the predicted surface pressure becomes more accurate in capturing the shock wave, and more smooth in the continuous region. The outperfromance of TCA over GFK can be observed in both interpolated and extrapolated cases. Besides, the standard multi-fidelity method is still better than the high-fidelity method. It should be noted that the performance of transfer learning (e.g., GFK over standard) can be different from the first two examples, since multiple input features have been included to model more complicated nonlinear dynamics. In the predicted pressure distributions, non-smoothness is observed, which comes for the linear superposition of high-fidelity POD modes [32]. In addition, the comparison of mean and standard deviation of the prediction error is shown in Table. 2, where the prediction accuracy is improved when transfer learning is used.

Since flow reconstruction focuses on flow details in the entire domain, the global flow field is reconstructed through Eq.(6) for a detailed comparison. The average root mean squared error distribution for all 9 test cases is compared in Fig.9. As shown in the figure, the error in surface pressure will also affect the reconstruction accuracy for the entire flow, and larger error is observed near the shock wave. Two transfer learning methods show similar accuracy with the smallest error. Taking a typical interpolated flow state at $(\alpha, Ma) = (5^{\circ}, 0.7850)$ as an example (a combination of high angle attack and high Mach number), Fig. 10 shows the reference flow field and the reconstructed flows from TCA and GFK, where both methods show good accuracy. Since the present methods rely on high-fidelity POD modes to reconstruct the pressure distribution, it may show large discrepancies for an extrapolation state at high angle attack and high Mach number, which requires either increasing the samples near these states or changing the reconstruction method. Further improvement of both transfer learning methods includes more systematic studies on kernel function selection and parameter settings.

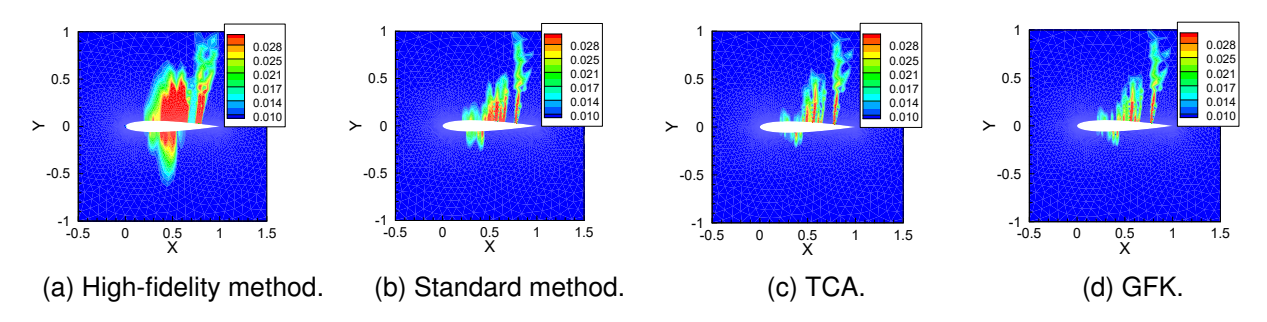


Figure 9 – Comparison of root mean squared error for transonic flow around a NACA0012 airfoil (9 test cases).

4.2 ONERA M6 Wing

In this section, transonic flow around a three-dimensional wing model is considered to further test the proposed transfer learning method for multi-fidelity flow reconstruction. The ONERA M6 wing

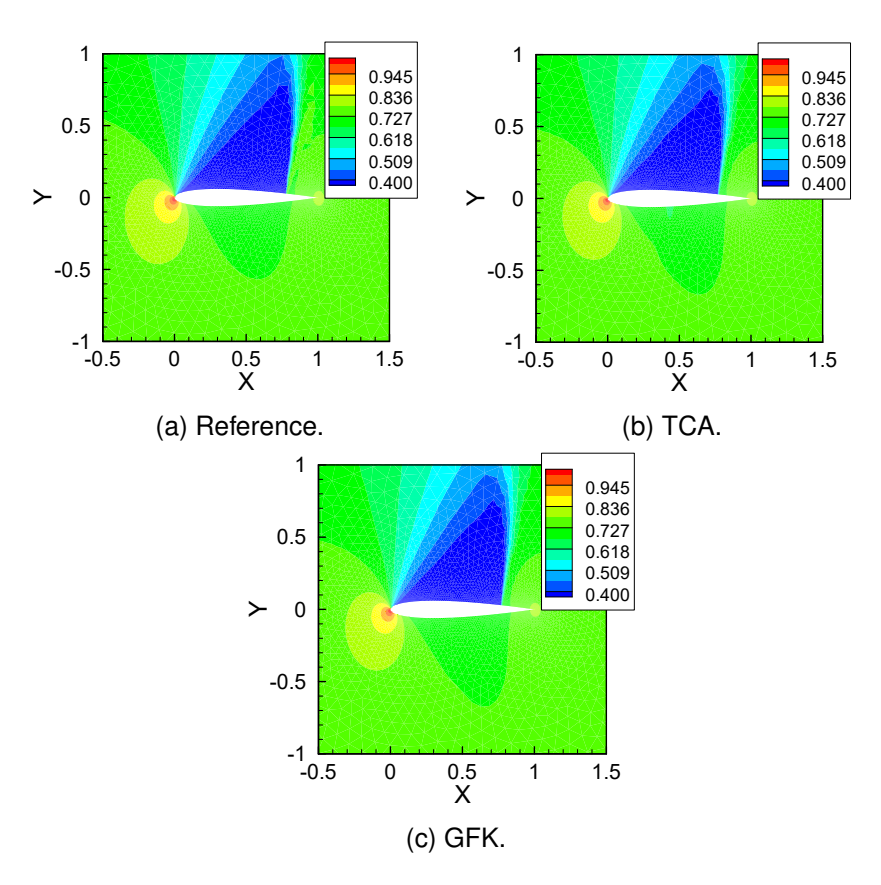


Figure 10 – Comparison of the predicted flow field for flow state at $(\alpha, Ma) = (5^{\circ}, 0.7850)$.

is selected, which is a classic swept-back wing model to test the accuracy of transonic flow simulation. To mimic viscous effects, Reynolds-Averaged Navier-Stokes (RANS) equations with the Spalart-Allmaras turbulence model [33] are solved based on the open source software SU2 [34]. The computational grid is obtained from the SU2 database, which contains 46417 nodes and 43008 hexahedral grids. The Reynolds number is set to 11.72×10^6 . Using the Cauchy error convergence criterion, the high-fidelity data is generated under a residual criterion of 1×10^{-6} while the low-fidelity data is generated under a residual criterion of 1×10^{-1} .

A uniform sampling method is chosen to sample the training cases in the parameter space. Similar to the previous case, the parameter space is composed of the angle of attack α and the Mach number Ma. The sampling ranges are $Ma \in [0.78, 0.84]$ and $\alpha \in [0^{\circ}, 5^{\circ}]$, where 28 samples are selected as shown in Fig. 11. Similar to the previous case, apart from two interpolation and one extrapolation cases, additional 3 test cases have been added to compute the prediction error and obtain error contours. With all six test cases, it is sufficient to fully evaluate the model performance. Since three-dimensional flows are more complicated with spanwise effects, the sampling range is smaller compared to the previous case. Two typical states $(\alpha, Ma) = (0.75^{\circ}, 0.835)$ and $(\alpha, Ma) = (4.25^{\circ}, 0.79)$ are chosen to test the interpolation performance of the proposed method, and one state outside the parameter space $(\alpha, Ma) = (3.5^{\circ}, 0.845)$ is used for extrapolation. Again, due to high dimension of the space, the surface pressure data are taken as the snapshot to reduce the numerical difficulty of the GFK method. The global flow field is recovered in the same way explained in Eq. (6). Eight typical spanwise positions y/b = 11.20%, 22.24%, 32.77%, 52.24%, 68.34%, 75.23%, 81.08%, 90.28% are sampled as the flow snapshot, where each slice contains 88 grid points, resulting in the snapshot dimension 704. Typical high-fidelity and low-fidelity snapshots at four spanwise positions and a particular state $(\alpha, Ma) = (4.0^{\circ}, 0.78)$ are compared in Fig. 12. The figure shows that low-fidelity simulation has some errors behind the shock wave, and the position and strength of the shock wave are also different.

Similar to the two-dimensional test case, for the high-fidelity method, the model input contains two state parameters, i.e., the angle of attack and the Mach number. For multi-fidelity modeling, multiple low-fidelity features are also used to predict the high-fidelity feature. Similar to previous sections, the

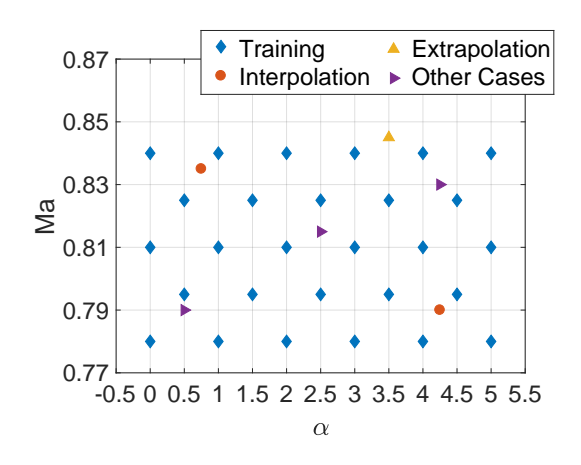


Figure 11 – Sampling space for transonic flow around the ONERA M6 wing.

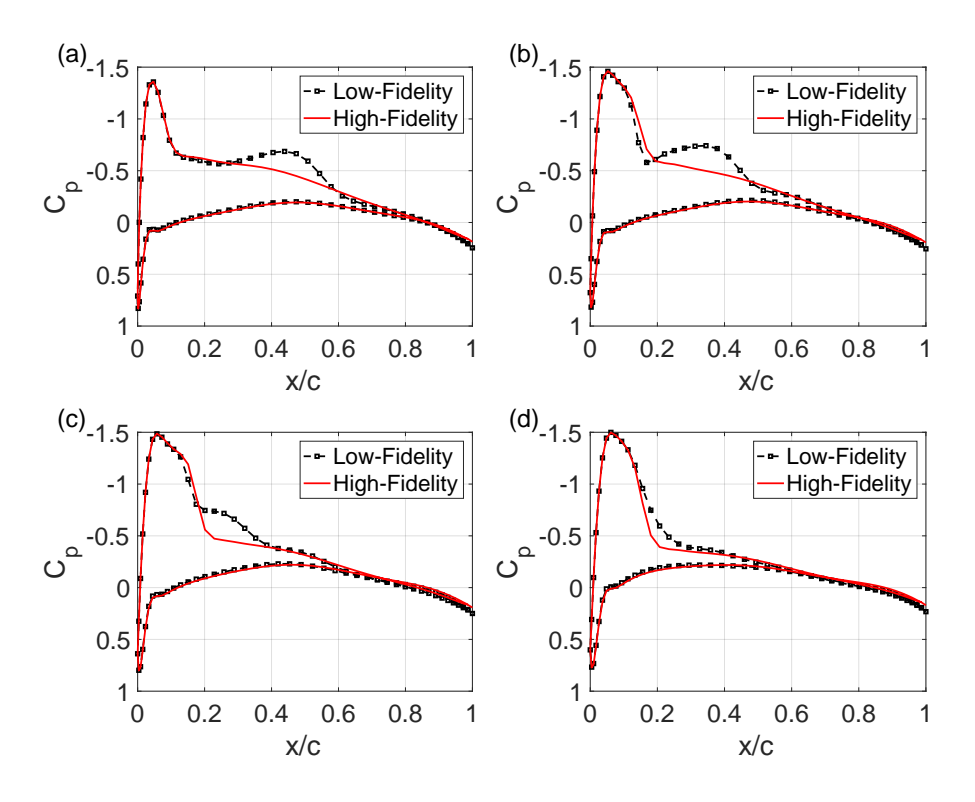


Figure 12 – Comparison of high-fidelity and low-fidelity surface pressure coefficients (ONERA M6 wing, $(\alpha, Ma) = (4.0^{\circ}, 0.78)$) (a) Spanwise position y/b = 22.24% (b) Spanwise position y/b = 52.24% (c) Spanwise position y/b = 75.23% (d) Spanwise position y/b = 90.28%.

Table 3 – Prediction error of surface pressure reconstruction by different methods (6 test cases, ONERA M6 wing).

Method	Mean	Standard Deviation
High-	8.7619×10^{-3}	1.5429×10^{-2}
Fidelity		
Standard	3.8038×10^{-3}	6.7070×10^{-3}
TCA	3.3139×10^{-3}	4.2867×10^{-3}
GFK	2.4917×10^{-3}	4.7629×10^{-3}

first 20 low-fidelity features are chosen for all three multi-fidelity methods to make a fair comparison and to show the capability of transfer learning in capturing high-order features. Again, TCA method selects the Gaussian kernel function to provide nonlinear mapping. The first 12 high-fidelity mode coefficients are predicted by the model. The reconstruction results of different methods for three test cases are shown in Fig.13, Fig.14 and Fig.15, respectively. These results clearly show that the challenge in such problems lies in the accurate reconstruction of shock waves. From the high-fidelity method, larger errors can be observed near the shock wave, which is better described by both standard and transfer learning methods. For the same number of input features, transfer learning outperforms the standard method, and improves the prediction near the shock wave. The mean and standard derivation of the prediction error is summarized in Table.3. Compared with the standard method, transfer learning reduces the prediction error both in terms of mean and standard derivation, indicating that more representative low-fidelity features are discovered to improve accuracy in multifidelity modeling for flow reconstruction.

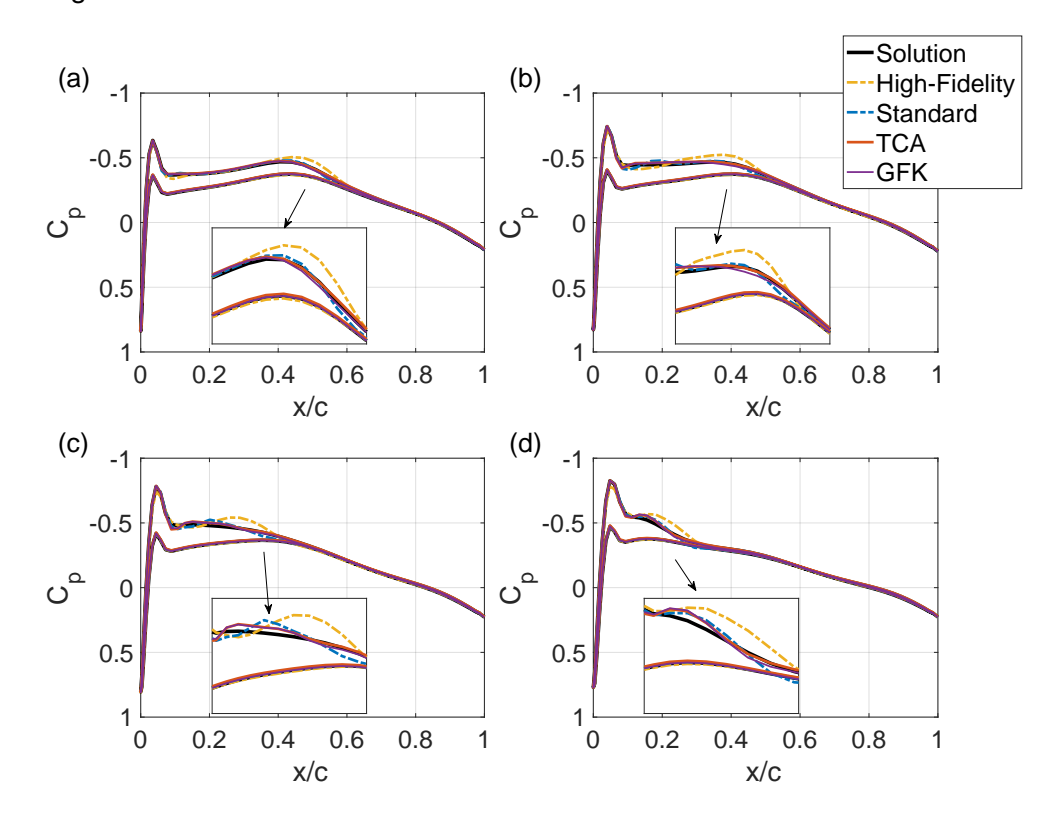


Figure 13 – Surface reconstruction comparison of interpolation test sample 1 (ONERA M6 wing, $(\alpha, Ma) = (0.75^{\circ}, 0.835)$) (a) Spanwise position y/b = 22.24% (b) Spanwise position y/b = 52.24% (c) Spanwise position y/b = 75.23% (d) Spanwise position y/b = 90.28%.

After reconstructing the entire field based on Eq. (6), the average root mean squared error contours

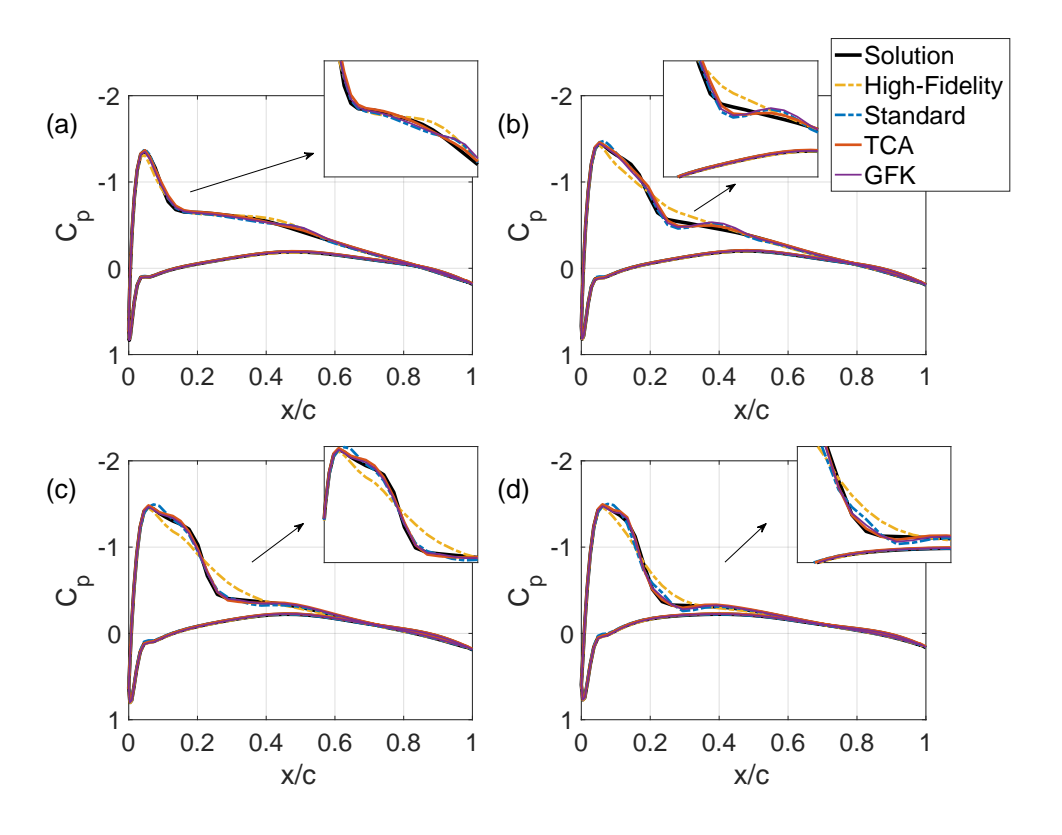


Figure 14 – Surface reconstruction comparison of interpolation test sample 2 (ONERA M6 wing, $(\alpha, Ma) = (4.25^{\circ}, 0.79)$) (a) Spanwise position y/b = 22.24% (b) Spanwise position y/b = 52.24% (c) Spanwise position y/b = 75.23% (d) Spanwise position y/b = 90.28%.

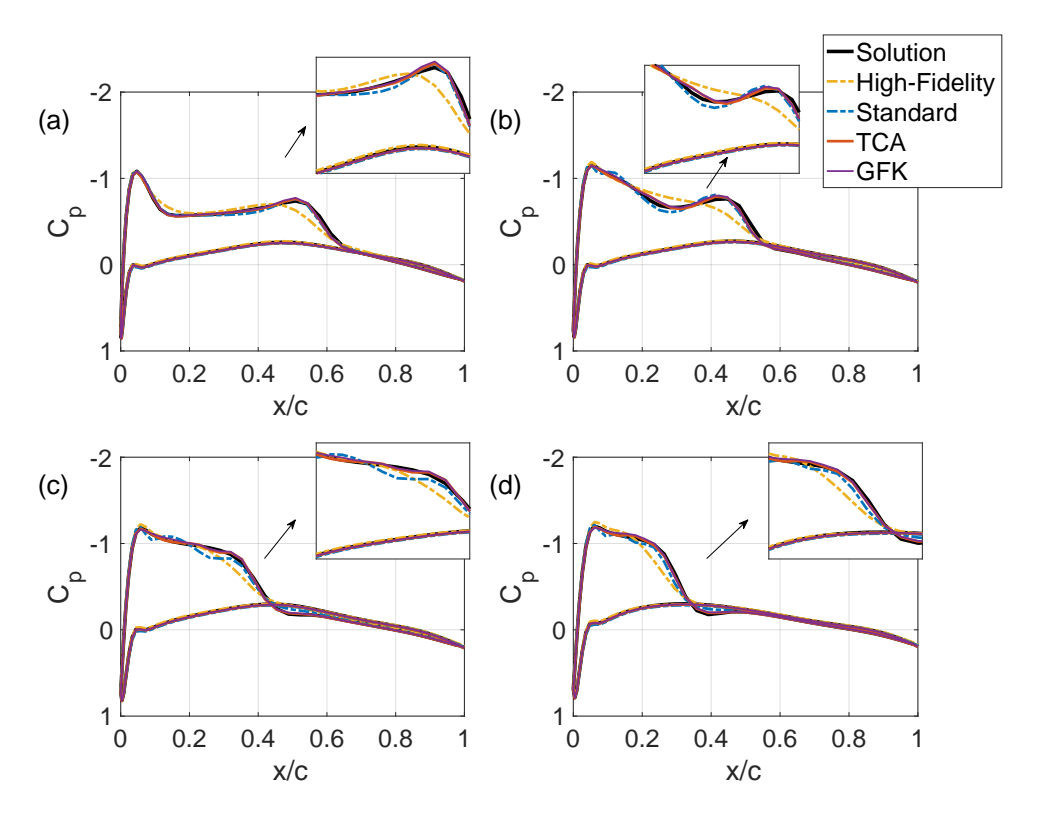


Figure 15 – Surface reconstruction comparison of extrapolation test sample (ONERA M6 wing, $(\alpha, Ma) = (3.5^{\circ}, 0.845)$) (a) Spanwise position y/b = 22.24% (b) Spanwise position y/b = 52.24% (c) Spanwise direction position y/b = 75.23% (d) Spanwise position y/b = 90.28%.

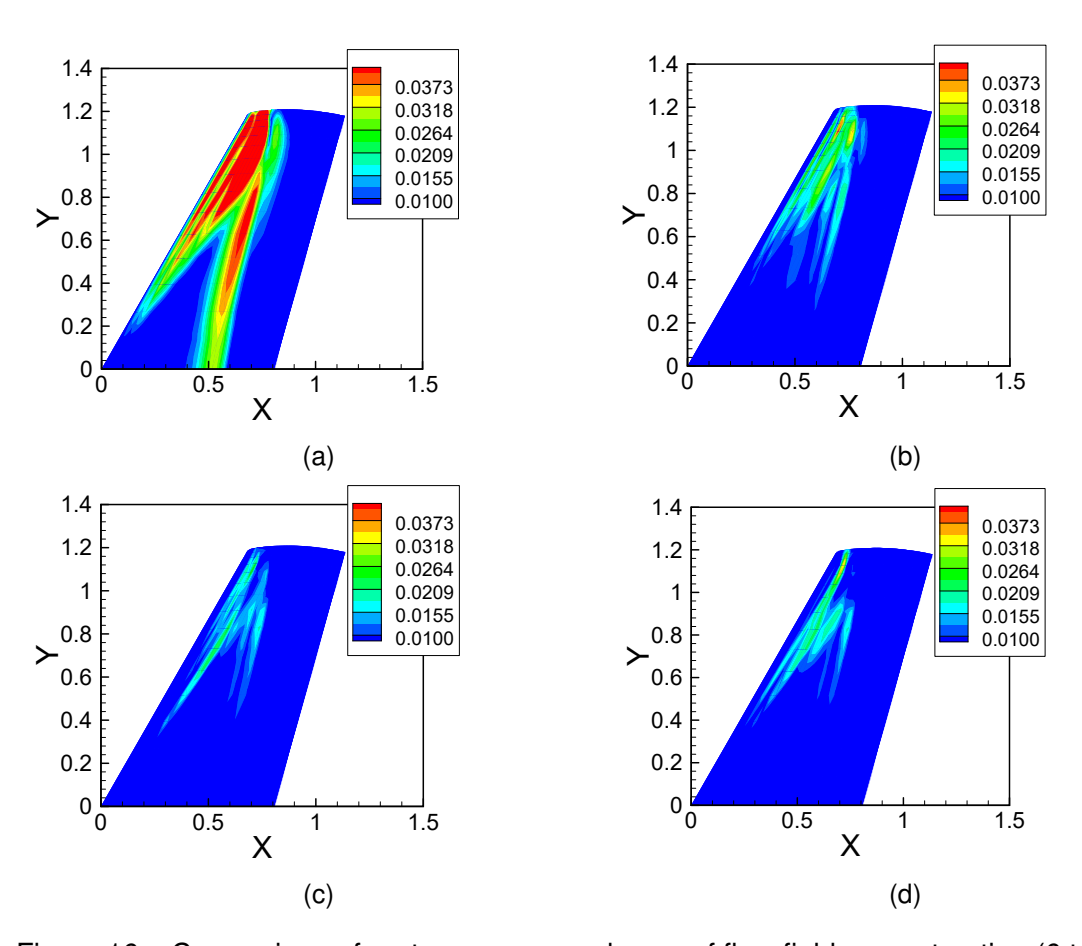


Figure 16 – Comparison of root mean squared error of flow field reconstruction (6 test cases, ONERA M6 wing) (a) High-fidelity method (b) Standard multi-fidelity method (c) TCA (d) GFK.

for all test cases are shown in Fig. 16. It can be observed that the errors are mainly concentrated in the vicinity of the Lambda-shaped shock waves. However, transfer learning only shows large errors near part of the shock. The reconstructed surface pressure for all methods and test cases is compared in Fig. 17, where both TCA and GFK follow the reference data more closely and the shock wave is predicted more accurately. It should be noted that the results from both transfer learning methods are mostly close to each other therefore is not distinguishable in the figure. In summary, all the test cases show the potential of transfer learning to discover representative features from multifidelity data that lead to improved accuracy in constructing multi-fidelity ROMs for flow reconstruction.

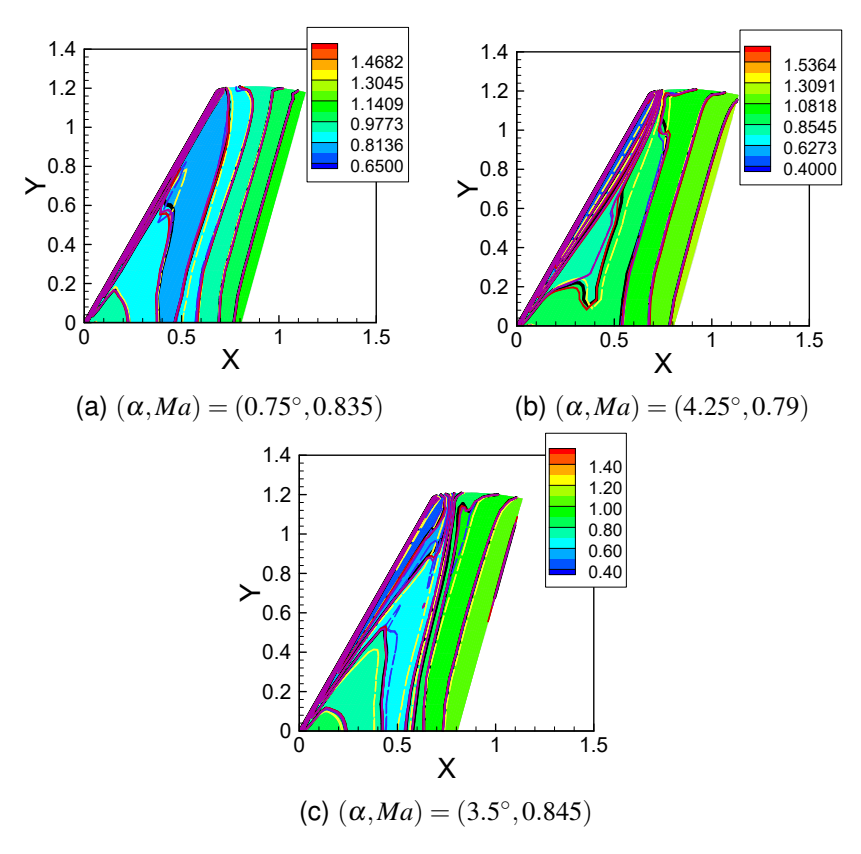


Figure 17 – Reconstructed surface pressure distribution for transonic flow around an ONERA M6 wing (black: reference solution; yellow: High-fidelity; blue: Standard; red: TCA; purple: GFK.).

4.3 Computational Cost

In this section, the computational cost of the proposed method is analyzed. The second test case (ONERA M6 wing), which is more of industrial interest, is investigated in detail. The simulation is performed on a workstation using a single Intel(R) Core(TM) i7-4770 CPU @ 3.40 GHz. For each high-fidelity simulation, about 45 minutes are needed, while each low-fidelity simulation takes about 3 minutes. For the training dataset with 28 samples, 1260 minutes and 84 minutes are needed for high-fidelity and low-fidelity simulations, respectively. The rest of cost is computed from the *tic-toc* function of MATLAB. As summarized in Table 4, the main cost of the proposed method lies in the generation of training data in the offline phase and the generation of low-fidelity data in the online phase. Compared to the high-fidelity method, multi-fidelity method increases the overall computational cost by about 8%, which mainly comes from the generation of low-fidelity data. In addition, it should also be noted that the computational cost of the GFK method scales with the size of snapshot matrix, therefore the snapshot with large size should be avoided in this method.

From the analysis, it can be observed that the cost of model training and model prediction is almost negligible, while the main source of additional cost for all multi-fidelity methods lies in generating the low-fidelity data. This also applies to other less complicated test cases involved in the present work. In the first test case (NACA0012 airfoil), low-order numerical scheme is used, which reduces the computational cost by about one third (from 7 minutes for high-fidelity simulation to 4.5 minutes

Table 4 – Approximation of computational cost for the last test case (ONERA M6 Wing), TL refers to transfer learning, LF refers to low-fidelity, recon. refers to reconstruction.

Model	Offline			Online			Time		
	Data	POD	TL	Train	LF runs	TL	Predict	Recon.	
High-Fidelity	1260min	0.02s	0	0.3s	0	0	0.05s	0.15s	1260.01min
Standard	1344min	0.04s	0	0.3s	10min	0	0.05s	0.15s	1354.01min
TCA	1344min	0.04s	0.1s	0.3s	10min	0.01s	0.05s	0.15s	1354.01min
GFK	1344min	0.04s	0.15s	0.3s	10min	0.015s	0.05s	0.15s	1354.01min

for low-fidelity simulation). Note that the cost can be further reduced when other low-fidelity simplifications are considered. Since the cost of each high-fidelity simulation remains relatively low, the overall cost of multi-fidelity methods is also reasonable compared to high-fidelity models. However, we would like to highlight again that the last test case is more realistic and more of industrial interest, which increases the computational cost very little (about 8%).

5. Conclusion

This paper proposes to use transfer learning for building reduced-order models that facilitate multifidelity flow reconstruction. The core concept involves employing transfer learning techniques to extract representative features that more accurately reflect the correlations between high-fidelity and low-fidelity data. Specifically, we utilize transfer learning approaches based on domain adaptation to enhance multi-fidelity flow reconstruction. We introduce two distinct frameworks for handling multifidelity flow data: TCA and GFK. TCA employs a nonlinear transformation to align the feature distributions of high- and low-fidelity data, while GFK is designed to identify a domain-invariant feature space that improves the correlation between the two data sets. Our preliminary tests, including complex scenarios like transonic flows around a NACA0012 airfoil and an ONERA M6 wing, underscore the benefits of our method in delivering enhanced accuracy, particularly in capturing the nonlinear dynamics of flows with shock waves. However, further refinements are necessary to improve the accuracy and smoothness of the predicted shock profiles. Future work will focus on refining our method through alternative kernel functions for TCA or nonlinear extensions for GFK, and applying our approach to more challenging cases where low-fidelity data significantly lacks physical details. Additionally, exploring ways to incorporate low-fidelity flow physics into model construction presents a valuable direction for future research.

6. Acknowledgments

This work was supported by the National Natural Science Foundation of China (No.12072282 and No.91852115).

7. Contact Author Email Address

The corresponding author email address is aeroelastic@nwpu.edu.cn (Weiwei Zhang) or you can contact the email address with jqkou@nwpu.edu.cn (Jiaqing Kou).

8. Copyright Statement

The authors confirm that they, and/or their company or organization, hold copyright on all of the original material included in this paper. The authors also confirm that they have obtained permission, from the copyright holder of any third party material included in this paper, to publish it as part of their paper. The authors confirm that they give permission, or have obtained permission from the copyright holder of this paper, for the publication and distribution of this paper as part of the ICAS proceedings or as individual off-prints from the proceedings.

References

[1] Earl H Dowell and Kenneth C Hall. Modeling of fluid-structure interaction. *Annual Review of Fluid Mechanics*, 33(1):445–490, 2001.

- [2] David J Lucia, Philip S Beran, and Walter A Silva. Reduced-order modeling: new approaches for computational physics. *Progress in aerospace sciences*, 40(1-2):51–117, 2004.
- [3] Jiaqing Kou and Weiwei Zhang. Data-driven modeling for unsteady aerodynamics and aeroelasticity. *Progress in Aerospace Sciences*, 125:100725, 2021.
- [4] S Ashwin Renganathan, Kohei Harada, and Dimitri N Mavris. Aerodynamic data fusion toward the digital twin paradigm. *AIAA Journal*, 58(9):3902–3918, 2020.
- [5] Benjamin Peherstorfer, Karen Willcox, and Max Gunzburger. Survey of multifidelity methods in uncertainty propagation, inference, and optimization. *Siam Review*, 60(3):550–591, 2018.
- [6] M Giselle Fernández-Godino, Chanyoung Park, Nam-Ho Kim, and Raphael T Haftka. Review of multi-fidelity models. *arXiv preprint arXiv:1609.07196*, 2016.
- [7] Jiaqing Kou and Weiwei Zhang. Multi-fidelity modeling framework for nonlinear unsteady aerodynamics of airfoils. *Applied Mathematical Modelling*, 76:832–855, 2019.
- [8] Xu Wang, Jiaqing Kou, and Weiwei Zhang. Multi-fidelity surrogate reduced-order modeling of steady flow estimation. *International Journal for Numerical Methods in Fluids*, 92(12):1826–1844, 2020.
- [9] Sinno Jialin Pan and Qiang Yang. A survey on transfer learning. *IEEE Transactions on knowledge and data engineering*, 22(10):1345–1359, 2009.
- [10] Lisa Torrey and Jude Shavlik. Transfer learning. In *Handbook of research on machine learning applications and trends: algorithms, methods, and techniques*, pages 242–264. IGI global, 2010.
- [11] Karl Weiss, Taghi M Khoshgoftaar, and DingDing Wang. A survey of transfer learning. *Journal of Big data*, 3(1):1–40, 2016.
- [12] Fuzhen Zhuang, Zhiyuan Qi, Keyu Duan, Dongbo Xi, Yongchun Zhu, Hengshu Zhu, Hui Xiong, and Qing He. A comprehensive survey on transfer learning. *Proceedings of the IEEE*, 109(1):43–76, 2020.
- [13] Sinno Jialin Pan, Ivor W Tsang, James T Kwok, and Qiang Yang. Domain adaptation via transfer component analysis. *IEEE transactions on neural networks*, 22(2):199–210, 2010.
- [14] Novi Patricia and Barbara Caputo. Learning to learn, from transfer learning to domain adaptation: A unifying perspective. In *Proceedings of the IEEE Conference on Computer Vision and Pattern Recognition*, pages 1442–1449, 2014.
- [15] Wouter M Kouw and Marco Loog. An introduction to domain adaptation and transfer learning. *arXiv preprint arXiv:1812.11806*, 2018.
- [16] Zhongwei Zhang, Huaihai Chen, Shunming Li, Zenghui An, and Jinrui Wang. A novel geodesic flow kernel based domain adaptation approach for intelligent fault diagnosis under varying working condition. *Neurocomputing*, 376:54–64, 2020.
- [17] Wouter M Kouw and Marco Loog. A review of domain adaptation without target labels. *IEEE transactions on pattern analysis and machine intelligence*, 43(3):766–785, 2019.
- [18] Boqing Gong, Yuan Shi, Fei Sha, and Kristen Grauman. Geodesic flow kernel for unsupervised domain adaptation. In *2012 IEEE conference on computer vision and pattern recognition*, pages 2066–2073. IEEE, 2012.
- [19] Tianzhu Liu, Xiangrong Zhang, and Yanfeng Gu. Unsupervised cross-temporal classification of hyperspectral images with multiple geodesic flow kernel learning. *IEEE Transactions on Geo*science and Remote Sensing, 57(12):9688–9701, 2019.

- [20] Jian Yu and Jan S Hesthaven. Flowfield reconstruction method using artificial neural network. *Aiaa Journal*, 57(2):482–498, 2019.
- [21] Christian Perron, Dushhyanth Rajaram, and Dimitri Mavris. Development of a multi-fidelity reduced-order model based on manifold alignment. In AIAA AVIATION 2020 FORUM, page 3124, 2020.
- [22] N Benjamin Erichson, Lionel Mathelin, Zhewei Yao, Steven L Brunton, Michael W Mahoney, and J Nathan Kutz. Shallow neural networks for fluid flow reconstruction with limited sensors. *Proceedings of the Royal Society A*, 476(2238):20200097, 2020.
- [23] Christian Perron. *Multi-Fidelity Reduced-Order Modeling Applied to Fields with Inconsistent Representations.* PhD thesis, Georgia Institute of Technology, 2020.
- [24] Margaret A Oliver and Richard Webster. Kriging: a method of interpolation for geographical information systems. *International Journal of Geographical Information System*, 4(3):313–332, 1990.
- [25] Søren Nymand Lophaven, Hans Bruun Nielsen, Jacob Søndergaard, et al. *DACE: a Matlab kriging toolbox*, volume 2. Citeseer, 2002.
- [26] Weiwei Zhang, Chuanqiang Gao, Yilang Liu, Zhengyin Ye, and Yuewen Jiang. The interaction between flutter and buffet in transonic flow. *Nonlinear Dynamics*, 82(4):1851–1865, 2015.
- [27] Yilang Liu, Weiwei Zhang, and Jiaqing Kou. Mode multigrid-a novel convergence acceleration method. *Aerospace Science and Technology*, 92:605–619, 2019.
- [28] Michael Stein. Large sample properties of simulations using latin hypercube sampling. *Technometrics*, 29(2):143–151, 1987.
- [29] Karen Willcox. Unsteady flow sensing and estimation via the gappy proper orthogonal decomposition. *Computers & fluids*, 35(2):208–226, 2006.
- [30] Saifon Chaturantabut and Danny C Sorensen. Nonlinear model reduction via discrete empirical interpolation. *SIAM Journal on Scientific Computing*, 32(5):2737–2764, 2010.
- [31] Xuan Zhao, Lin Du, Xuhao Peng, Zichen Deng, and Weiwei Zhang. Research on refined reconstruction method of airfoil pressure based on compressed sensing. *Theoretical and Applied Mechanics Letters*, page 100223, 2021.
- [32] Jing Li and Weiwei Zhang. The performance of proper orthogonal decomposition in discontinuous flows. *Theoretical and Applied Mechanics Letters*, 6(5):236–243, 2016.
- [33] Philippe Spalart and Steven Allmaras. A one-equation turbulence model for aerodynamic flows. In 30th aerospace sciences meeting and exhibit, page 439, 1992.
- [34] Thomas D Economon, Francisco Palacios, Sean R Copeland, Trent W Lukaczyk, and Juan J Alonso. Su2: An open-source suite for multiphysics simulation and design. *Aiaa Journal*, 54(3):828–846, 2016.